13. S. Y. Chung, M. Yoon, and D. E. Kim, "Generation of attosecond x-ray and gamma-ray via Compton backscattering," Opt. Express **17**(10), 7853–7861 (2009).
14. A. A. Zholents and W. M. Fawley, "Proposal for intense attosecond radiation from an x-ray free-electron laser," Phys. Rev. Lett. **92**(22), 224801 (2004).
15. A. A. Zholents, "Method of an enhanced self-amplified spontaneous emission for x-ray free electron lasers," Phys. Rev. ST Accel. Beams **8**(4), 040701 (2005).
16. A. A. Zholents and M. S. Zolotorev, "Attosecond x-ray pulses produced by ultra short transverse slicing via laser electron beam interaction," N. J. Phys. **10**(2), 025005 (2008).
17. A. A. Zholents and G. Penn, "Obtaining attosecond x-ray pulses using a self-amplified spontaneous emission free electron laser," Phys. Rev. ST Accel. Beams **8**(5), 050704 (2005).
18. E. L. Saldin, E. A. Schneidmiller, and M. V. Yurkov, "A new technique to generate 100 GW-level attosecond x-ray pulses from the x-ray SASE FELs," Opt. Commun. **239**(1–3), 161–172 (2004).
19. E. L. Saldin, E. A. Schneidmiller, and M. V. Yurkov, "Terawatt-scale sub-10-fs laser technology –key to generation of GW-level attosecond pulses in x-ray free electron laser," Opt. Commun. **237**(1-3), 153–164 (2004).
20. R. Bonifacio, L. D. S. Souza, P. Pierini, and E. T. Scharlemann, "Generation of XUV light by resonant frequency tripling in a two-wiggler FEL amplifier," Nucl. Instrum. Methods Phys. Res. A **296**(1-3), 787–790 (1990).
21. L. H. Yu, "Generation of intense uv radiation by subharmonically seeded single-pass free-electron lasers," Phys. Rev. A **44**(8), 5178–5193 (1991).
22. J. Wu and L. H. Yu, "Coherent hard x-ray production by cascading stages of high gain harmonic generation," Nucl. Instrum. Methods Phys. Res. A **475**(1-3), 104–111 (2001).
23. E. Allaria and G. De Ninno, "Soft-x-ray coherent radiation using a single-cascade free-electron laser," Phys. Rev. Lett. **99**(1), 014801 (2007).
24. G. Stupakov, "Using the beam-echo effect for generation of short-wavelength radiation," Phys. Rev. Lett. **102**(7), 074801 (2009).
25. D. Xiang and G. Stupakov, "Echo-enabled harmonic generation free electron laser," Phys. Rev. ST Accel. Beams **12**(3), 030702 (2009).
26. Laser acceleration-focused laser *http://www.slac.stanford.edu/~achao/LaserAccelerationFocussed.pdf*.
27. H.-S. Kang and S.-H. Nam, in Proceedings of the 32nd International FEL 2010 Conference (Malmo, Sweden, Aug. 23–27, 2010), *http://fel2010.maxlab.lu.se/*.
28. M. Borland, "Elegant: A flexible SSD-compliant code for accelerator simulation," *http://www.aps.anl.gov*.
29. S. Reiche, "GENESIS 1.3: a fully 3D time-dependent FEL simulation code Nucl. Instrum. Methods Phys. Res. A **429**, 243–248 (1999), *http://pbpl.physics.ucla.edu/~reiche/*.

1. Introduction

Attosecond science is to measure, control and ultimately manipulate attosecond time-scale electron dynamics in matter. These dynamics determine how physical and chemical changes occur at a fundamental level. To study these dynamics we need an isolated single pulse in attosecond time scale. The recent research has confirmed and has shown that it is indeed possible to generate a single isolated pulse of attosecond duration [1–7] and moreover its applications [8–10] has opened a door to the investigation of ever faster processes in nature such as electronic transitions in atoms and molecules that have never been explored before.

To achieve atomic spatial resolution, the radiation wavelength needs to be pushed to ~0.1 nm or shorter; consequently an isolated attosecond pulse at 0.1 nm or shorter is highly desirable for attosecond temporal resolution and nanometer spatial resolution. During the last decade, an isolated attosecond XUV pulse has been successfully produced using the high-harmonics generation (HHG) method from a neutral gas [3–10] in the soft x-ray region. For hard x-rays, ideas using Thomson scattering [11,12], Compton backscattering [13] and free electron laser (FEL) have been proposed.

In FEL there are two leading schemes; one is self-amplified spontaneous emission (SASE) scheme [14–19] and other is the high gain harmonic generation (HGHG) scheme [20–25]. A free electron laser based upon the principle of SASE has been considered as a potential source of obtaining femtosecond (fs), short wavelength x-ray pulses. But the problem lies in limited temporal coherence of the output radiation of a SASE FEL. Moreover, this radiation consists of many sub-fs "spikes" whose arrival time is random on a shot-to-shot basis. This prevents the straightforward use of SASE FEL in pump probe experiments at the attosecond time scale.

The introduction of a conventional optical laser to SASE FEL scheme could enhance the electron peak current, thereby leading to the considerable reduction in jitter and the FEL length. This is called enhanced SASE (ESASE) scheme. The ESASE technique [15] employs an optical laser to induce energy modulation in an electron bunch to create a strong current peak of a short duration. This leads to the generation of short duration ($\tau < 500$ attosecond)

output pulses from an FEL together with the absolute synchronization of x-ray probe pulses to laser pump pulses, allowing for pump-probe experiments. Up to now, all the works cited above produces a train of attosecond pulses. This may be not so useful for experiments with attosecond temporal resolution.

In this paper, we demonstrate that an isolated attosecond pulse can be indeed produced by manipulating electron-beam energy distributions together with density modulation in ESASE scheme for a given laser wavelength. An optical laser with a high intensity is used for the energy modulation of a relativistic electron bunch inside a wiggler. This energy-modulated electron bunch is further compressed by the chicane of four dipole-magnets. The FWHM pulse duration, electron-bunch energy distributions are optimized to control the side current-peaks and to obtain single isolated attosecond pulse.
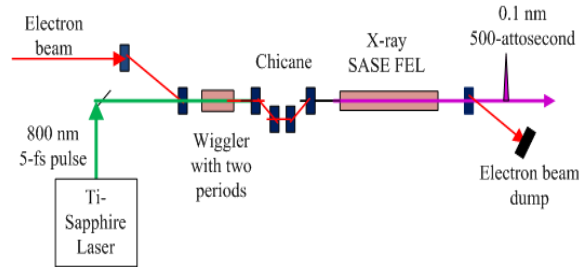
2. Method

Fig. 1. ESASE scheme for attosecond pulse generation.

Figure 1 shows a schematic of the ESASE scheme considered in this study. An electron beam exits from a linear accelerator and is sent to a double-period wiggler magnet. At the same time, a co-propagating few-cycle carrier envelop-phase (CEP) stabilized laser is used to further induce the electron energy modulation inside the double-period wiggler. This wiggler magnet acts as an energy modulator. Only a small longitudinal section of the electron beam interacts with the laser and emerges from the wiggler with energy modulation. The peak power of the laser is selected in such a way that the amplitude of energy modulation significantly exceeds the uncorrelated energy spread of the electrons. The electron beam now enters a chicane, which introduces dispersion. This is a set of four magnets arranged in the configuration shown in Fig. 1. Here higher-energy electrons travel a shorter path and lower-energy electrons travel a longer path. In general this leads to the density modulation, producing microbunching of the electrons at laser wavelength spacing and periodic enhancement of the peak current. The increase in the peak current is accompanied by a corresponding increase in the energy spread of electrons. Finally the electron-bunch enters a long undulator to produce perfect microbunches and radiation at x-ray wavelength via standard SASE process.

For this analysis, the laser has the lowest Gaussian eigenmode TEM_{00} (Transverse Electro Magnetic) with zero offset [26]. We consider a planar wiggler,

$$\begin{cases} B_y = B_0 \cos k_w z \\ B_z = 0 \end{cases} \tag{1}$$

where $k_w = 2\pi/\lambda_w$ and λ_w is the wiggler period. The FEL resonance condition $\lambda_L = \left(\lambda_w/2\gamma_w^2\right)\left(1 + K_w^2/2\right)$ is maintained for the better energy exchange between the laser and electron beam. λ_L is the laser wavelength and γ_w the relativistic factor of the electron beam inside the wiggler, K_w the wiggler parameter, $K_w = eB_0\lambda_w/2\pi mc$, where m, e are the electron mass and charge, c the speed of light, and B_0 the peak magnetic field.

Due to SASE process in an undulator of λ_u and undulator parameter $K_r = eB_r\lambda_u/2\pi mc$, where B_r is the peak magnetic field, x-rays at a wavelength of $\lambda_r = \left(\lambda_u/2\gamma_r^2\right)\left(1 + K_r^2/2\right)$ is produced, where γ_r is the relativistic factor for the electron beam energy inside undulator.

As mentioned, the electron bunch is modulated in energy via interaction with a laser, and then, in density by a chicane. These are shown in Fig. 2. Figure 2(a)–2(c) show the longitudinal energy distribution of a 20 μm long (average-current 3 kA) electron bunch before wiggler, after wiggler and after chicane, respectively.
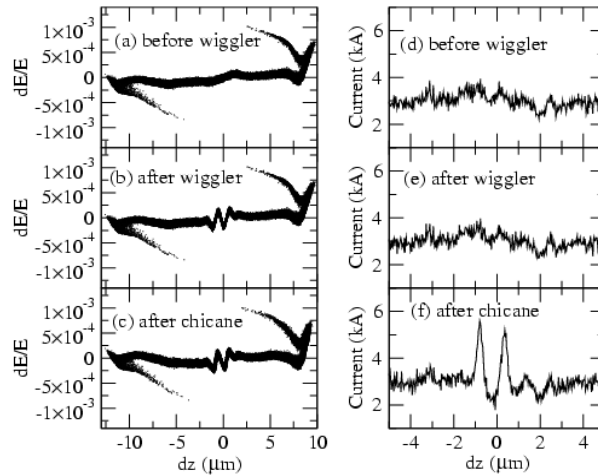

Fig. 2. The longitudinal energy distribution [(a), (b), (c)] and instantaneous current profile (d), (e), (f)] of electron bunch along the bunch length before wiggler, after wiggler, and after chicane. The average current is 3 kA and the bunch length is ~20 μm. The simulation has been done with a laser power 13 GW, λ_L = 1200 nm and 7.5 fs FWHM pulse duration.

One can see from Fig. 2(a) that before wiggler, there is a small energy-spread in the central region of electron bunch; after interacting with a laser, the energy modulation resembling the oscillation of the laser field is introduced as shown in Fig. 2(b). As shown in Fig. 2(c), this modulation becomes steeper by chicane. This is manifested as current spikes in the current profile of the electron bunch as shown in Fig. 2(f). The energy spread is always kept less than FEL parameter ($\Delta E/E < 5.4 \times 10^{-4}$) by adjusting the laser power. The corresponding current-profiles are shown in Fig. 2(d)–2(f), respectively. The current profile at wiggler entrance and after wiggler look similar in magnitude and shape [Fig. 2(d) and 2(e)] but after chicane there are two enhanced spikes in the central region of electron bunch; one spike of 5.6 kA at - 0.8 μm position and other spike of 5 kA at 0.36 μm. The increase in the peak current in the central region in Fig. 2(f) is caused due to the steepening of $\Delta E/E$ profile in the energy spread of electrons [see Fig. 2(c)].

3. Simulation results

For our calculations we consider an electron beam with parameters similar to those of the electron beam of Korean X-ray FEL [27]: a beam-energy of 10 GeV, (i.e. relativistic factor $\gamma \cong 2\times10^4$), a total electron bunch-charge is 0.2 nC. The electron bunch is 12 μm (≈ 40 fs) long with a normalized emittance of 0.5 μm-rad, a rms energy spread of 1 MeV. We consider an 800 nm, 26 GW power and 5 fs FWHM laser for energy modulation of the electron bunch. The laser is CEP stabilized. The laser is focused to a beam-waist of 250 μm at the center of wiggler. The magnetic field inside the wiggler is described by Eq. (1) with B$_0$ = 1.1459 T and λ_w = 55 cm. The momentum compaction factor $R_{56} \approx -2\theta_B^2\left(L_1 + 2/3L_B\right)$ for the

chicane magnet is 0.6 mm where θ_B, the bending angle of the dipole, is equal to 0.48°, $L_1 = 4$ meter is the drift length between the first and second dipole magnet and also the length between third and fourth dipole magnet and the associated dipole length of each dipole magnet is $L_B = 0.3$ meter. The electron beam properties at the entrance of undulator are calculated by Elegant code [28]. Elegant code is a six dimensional accelerator program used to generate particle distribution and track it.

We have run a number of simulations for the electron-beam modulation for different laser wavelengths, pulse durations and energy distributions of electron bunch. We found out that the modulation of electron bunch is sensitive to these parameters. This can be observed in longitudinal energy distribution, current-profile and normalized-emittance of electron-beam before wiggler, after wiggler and after chicane.

3.1 Dependence of current profile of electron bunch on laser parameters

We consider laser wavelengths in the range of 800 nm to 2400 nm with FWHM pulse durations of 5 fs to 14 fs. The electron-beam parameters were described in the above.
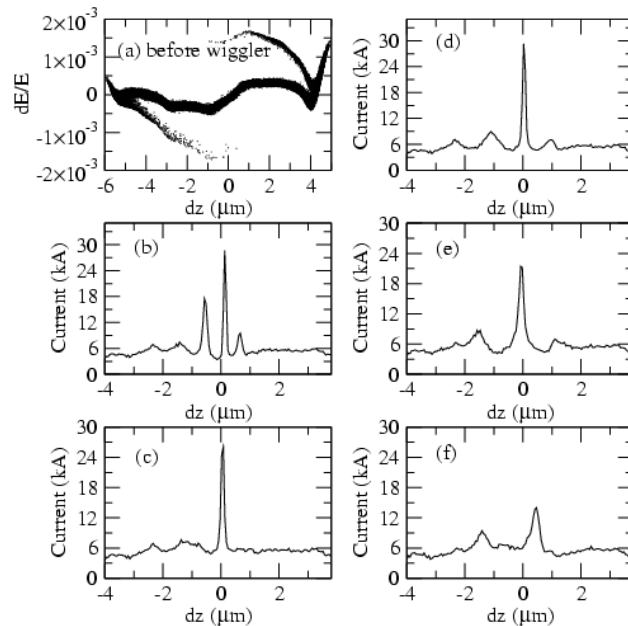

Fig. 3. (a) The longitudinal energy distribution of electron bunch before wiggler; (b) - (f), the current profile after chicane for different laser parameter, (b) $\lambda_L = 800$ nm & τ (FWHM) = 5 fs, (c) $\lambda_L = 1200$ nm & τ (FWHM) = 5 fs, (d) $\lambda_L = 1200$ nm & τ (FWHM) = 7.5 fs, (e) $\lambda_L = 1600$ nm & τ (FWHM) = 10 fs, (f) $\lambda_L = 2200$ nm & τ (FWHM) = 14 fs. The laser power is 26 GW. The average current is 6 kA and total bunch length is ~12 μm.

Figure 3(a) shows the longitudinal energy distribution of the electron bunch before the wiggler. In Fig. 3(b)–3(f), we present the current-profiles after chicane for different laser wavelengths. For $\lambda_L = 800$ nm and a pulse width of $\sqrt{2\pi}\sigma_{rms} = 5$ fs FWHM [Fig. 3(b)], note that there are three spikes in the central region of the electron bunch, generated by energy modulation and density modulation. The magnitude of the first spike is 17 kA at a position of - 0.57 μm along the bunch; that of the second spike is 28 kA at a position of 0.129 μm and the third spike is at a 9 kA at position of 0.66 μm. The background current is 6 kA. The contrast ratio between the first, second and third spike is 1.88: 3.1: 1 approximately, which is not good for producing a single pulse in FEL output.

In Fig. 3(c), we choose another wavelength 1200 nm with 5 fs FWHM. The simulation results show a single current spike of magnitude 26 kA at 0.0811 μm position and almost

vanishing side spikes. This result gives a substantially higher contrast ratio of 4.33: 1 between the central spike and the side peak above the background current. Similarly, in Fig. 3(d) for 1200 nm wavelength and 7.5 fs FWHM laser, we get the main current spike of 29 kA at 0.0273 μm with two side spikes with lower magnitudes of 8.96 kA and 7 kA at −1.1 μm and 0.99 μm, respectively. The contrast ratio among these spikes is around 1.28: 4.14: 1. For 1600 nm wavelength and 10 fs FWHM laser [see Fig. 3(e)] we get two spikes with current 8.7 kA and 21 kA at −1.57 μm and −0.073 μm with contrast ratio 2.4:1. For 2200 nm wavelength and 14 fs FWHM [see Fig. 3(f)], we again get an additional side spike of 9.43 kA at −1.41 μm and the main current spike of 14 kA at 0.4699 μm with contrast ratio 1:1.48. We have done similar calculations for other wavelengths, which we do not show here. Finally, we find that 1200 nm wavelength and 5 fs FWHM candidate seems the best with good contrast ratio. Nevertheless technically the generation of such a laser pulse is challenging. Now we consider 1200 nm wavelength and 7.5 fs FWHM laser. For this case, the contrast ratio of the main current spike to the side spikes is better compared with that for other examples.
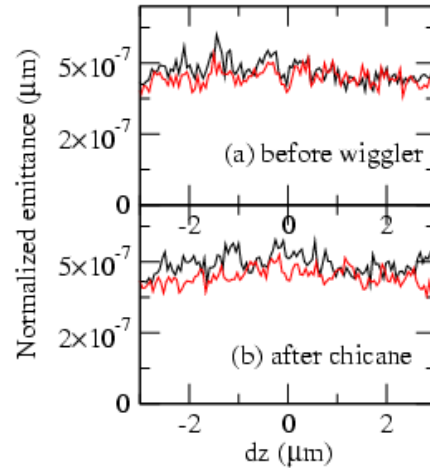

Fig. 4. Normalized horizontal emittance (black line) and vertical emittance (red line) of the electron bunch along the bunch length, (a) before wiggler, (b) after the chicane. The average current is 6 kA and total bunch length is ~12 μm. The laser power is 26 GW, λ_L = 1200 nm and 7.5 fs FWHM pulse duration.

With respect to the change of the emittance through the wiggler and chicane, we present the normalized emittance of electron bunch in a plane perpendicular the propagation direction of the electron bunch. In Fig. 4(a) and 4(b), the normalized emittance is shown before wiggler and after chicane. One can see from Fig. 4(b) that normalized emittance in the central region of electron bunch does not have a significant degradation due to the energy modulation by laser beam.

3.2 Dependence of current profile of electron bunch on the energy distribution

An alternative to control the side peaks in current-profile is to manipulate electron-bunch energy distribution. Different energy distributions of electron bunch can be produced by changing the RF phase in the linear acceleration column and adjusting the chicane parameters of the bunch compressors.

We have carried out a series of simulations for three different distributions of electron bunch energy: (1) approximately 20 μm ($\approx$ 66 fs) and average beam current 3 kA, (2) 16 μm ($\approx$ 53 fs) and 4 kA (3) 12 μm ($\approx$ 40 fs) and 6 kA. The total number of electrons is kept the same in all three distributions. Other electron bunch parameters are the same as given in section 3. Now we fix the laser parameters: 13 GW power, 1200 nm wavelength and 7.5 fs (FWHM) pulse duration. The ESASE parameters used are λ_w = 55 cm, K_w = 58, B_0 = 1.1459 T. The momentum compaction factor R_{56} is optimized between good quality of

electron-beam and the size of chicane. The momentum compaction parameter R_{56} used is 0.5 mm. The first case has already been presented to explain the ESASE mechanism (see Fig. 2). Here we will present the second and third case.
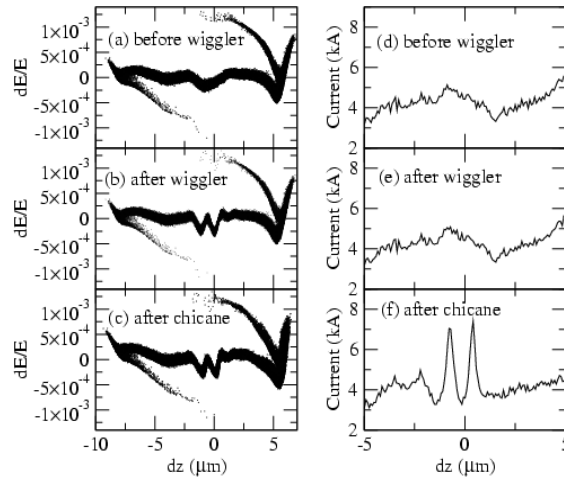

Fig. 5. The longitudinal energy distribution [(a), (b), (c)] and instantaneous current profile [(d), (e), (f)] along the bunch length before wiggler, after wiggler, and after chicane. The average current is 4 kA and the bunch length is ~16 μm. The laser power is 13 GW, λ_L = 1200 nm and 7.5 fs FWHM pulse duration.

Figure 5 shows the simulation results for the electron bunch with a length of 16 μm and an average current of 4 kA. Figure 5(a) and 5(d), Fig. 5(b) and 5(e), and Fig. 5(c) and 5(f) show the longitudinal energy distribution and current profile of the bunch before, after wiggler and after chicane, respectively. The energy distribution is well modulated due to the interaction with a laser in the wiggler [Fig. 5(b)]. The oscillations of the laser field are well replicated in energy distribution. The energy modulation in the central cycle of the laser is much stronger than in other cycles. However, we note that there is almost no difference in current profile before & after the wiggler [Fig. 5(c)]. The chicane plays a significant role; the rising slope becomes steeper [Fig. 5(c)] and two current spikes appears [Fig. 5(f)]. After chicane, the current profile has two current-spikes with magnitude 7 kA and 7.39 kA at −0.78 μm and 0.4 μm, respectively.

On the next page, Fig. 6 shows the results from the simulations for the bunch of 12 μm length (≈ 40 fs). The average current is 6 kA. The energy distribution of this electron bunch [Fig. 6(a)] is different from that in Fig. 5(a) because this bunch is pre-modulated in linear accelerator section. This pre-modulated electron bunch is now again modulated in a wiggler by 1200 nm and 7.5 fs laser [Fig. 6(b)) and then further compressed by the magnetic chicane [Fig. 6(c)].
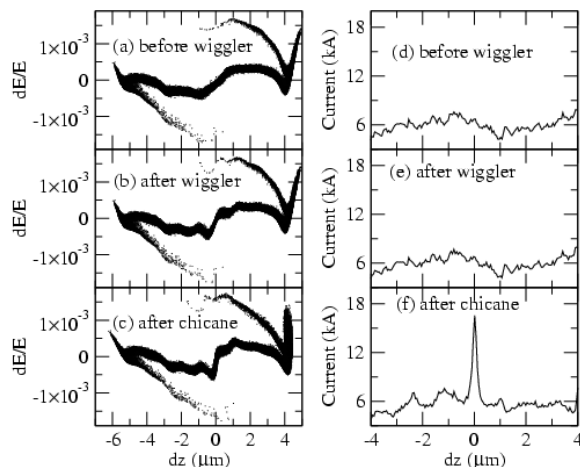
Fig. 6. The longitudinal energy distribution [(a), (b), (c)] and instantaneous current profile [(d), (e), (f)] along the bunch length before wiggler, after wiggler and after chicane. The average current of electron bunch is 6 kA and the bunch length is ~12 μm. The laser power is 13 GW, λ_L = 1200 nm and 7.5 fs FWHM pulse duration.

As shown in Fig. 6(f), there is only one current-spike of 17 kA at 0.013 μm and side peaks almost disappear, compared to Fig. 2(f) and 5(f). This demonstrates that by the manipulation of the energy distribution of electron bunch, one can minimize the side peaks in the interaction of laser and electron bunch so that an isolated current peak is generated. The FWHM duration of this current-spike is one femtosecond, which will become even shorter during the passage through the undulator.

4. Generation of isolated attosecond x-ray pulse

The electron bunch after the chicane is fed into a 100 meter long undulator. The radiation produced by these modulated electron bunches in the undulator is computed by a three-dimensional time- dependent FEL code GENESIS [29]. The undulator is planar with a period of 2.7 cm, a undulator gap of 4 mm, a undulator parameter of A_{w0} = 1.57 and 48 cm long break sections used for the quadrupoles at every 4.3 meter providing electron beam focusing with beta function β_x, β_y = 20 meter. The number of undulator periods for a 34 meter long undulator is 34 m / 2.7 cm = 1259, and the total slippage distance is 1259 × 0.1 nm = 125.9 nm = 0.4 fs. The output radiation at 0.1 nm x-ray wavelength has been calculated.

We present x-ray radiation produced by a 12 μm long electron bunch as shown in Fig. 3(a). A 1200 nm and 7.5 fs FWHM laser [see current profile in Fig. 3(d)] have modified this bunch. On the next page, Fig. 7(a) shows the logarithmic plot of the radiation power along the propagation direction when the electron bunch propagates z = 34 meter of the undualtor. The inset of Fig. 7(a) shows the same radiation power in a linear scale. The pulse duration of this peak is ~146 attosecond FWHM and the typical peak power is ~58 GW, which is averaged over beam slices. Figure 7(b) shows the x-ray output power from the strong current spike and two closest weak side spikes as a function of distance along the FEL. As shown in Fig. 3(d), there are three current spikes of magnitude 8.96 kA, 29 kA and 7 kA, respectively. The radiation from the strong current spike with 29 kA peak current, which has approximately 450 attosecond FWHM in Fig. 3(d), reaches saturation at a undulator length of 34-m [red line in Fig. 7(b)]. The saturation length is defined as the point where the linear growth of the radiation power gain stops. After 34 meter distance, roughly 33 GW power is maintained in this pulse. Another key quantity for high-gain FEL is the gain length, the length in which the FEL power grows by a factor e (= 2.718). As noticed in Fig. 7(b), the radiation from main peak demonstrates, at best, a gain length of 2 meter until it reaches saturation levels after

passing through ~34 meter of the FEL. After this point, the radiation power produced by the main current spike grows very slowly, because the slippage lengthens the pulse width. The closest side peaks, 1 μm away from the main peak [see Fig. 3(d)], have gain length 6 meter and 5 meter, respectively. The saturation lengths for these side peaks are 55 meter and 45 meter, and the corresponding peak power is 2.4 GW and 7.9 GW, respectively. As we note, the radiation power produced by the main peak is by two orders of magnitude greater than the power produced by side peaks.

Here space charge effects of the electron beam in GENESIS simulation are neglected. At this energy, effects of space charge force are not important. The effect of the space charge forces at injector section has been taken into account. However, we simulated our results using space charge effects in GENESIS simulation and we find that it does not give any difference.
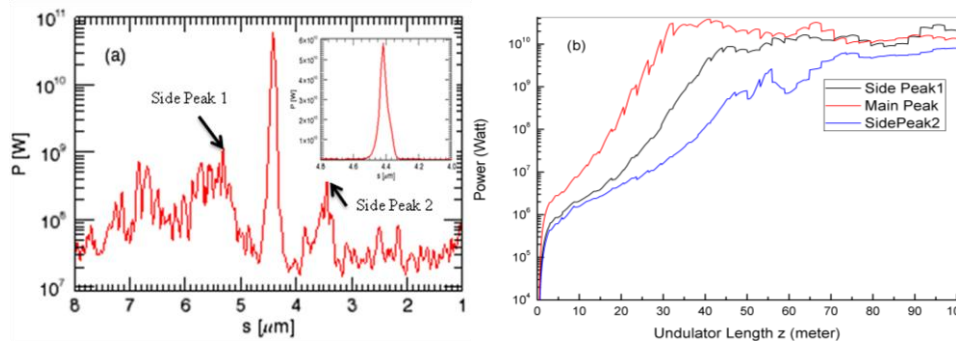

Fig. 7. (Color online) Atto-second XFEL of 0.1 nm SASE output: (a) radiation power (averaged over beam slices) versus electron-bunch length at z = 34 meter (inset figure shows main peak power in a linear scale), (b) maximum radiation power due to main peak and two side peaks along undulator length.

5. Summary

There is a growing demand for the generation of an isolated attosecond pulse in a hard x-ray region (a few ten keV). In this paper, we clearly demonstrate that such a pulse can be produced in ESASE by either optimizing laser parameters (wavelength and pulse durations) or manipulating the energy distribution of electron bunch or both. Through the optimization for laser wavelengths and pulse durations we find that 1200 nm and 7.5 fs FWHM are optimal laser parameters for producing a single attosecond current spike with a high contrast ratio in a 10 GeV electron beam. An alternative method is the manipulation of electron energy distribution. We have considered three different energy distributions and lengths. We demonstrated that single attosecond current spike can also be produced and such a current spike produces isolated attosecond x-ray pulse in an undualtor. An isolated 146 attosecond, 58 GW peak-power x-ray pulse at 0.1 nm is expected to be produced in a 34 meter long undulator for a driving laser of 1200 nm, 7.5 fs FWHM, and 0.2 mJ and Korean XFEL electron bunch. This isolated attosecond hard x-ray pulse will add a new dimension to attosecond pump-probe experiment in the study of electron dynamics.